Review Article

Ultrashort time to echo magnetic resonance techniques for the musculoskeletal system

Palanan Siriwanarangsun[1,2], Sheronda Statum[1,3], Reni Biswas[1,3], Won C. Bae[1,3], Christine B. Chung[1,3]

[1]Department of Radiology, University of California, San Diego, La Jolla, CA, USA; [2]Department of Radiology, Faculty of Medicine Siriraj Hospital, Mahidol University, Bangkok, Thailand; [3]Department of Radiology, VA San Diego Healthcare System, San Diego, CA, USA

Correspondence to: Christine B. Chung, M.D. Radiology Service, University of California San Diego, 9427 Health Sciences Drive, Mail Code 0997, La Jolla, CA 92093, USA. Email: cbchung@ucsd.edu.

Abstract: Magnetic resonance (MR) imaging has been widely implemented as a non-invasive modality to investigate musculoskeletal (MSK) tissue disease, injury, and pathology. Advancements in MR sequences provide not only enhanced morphologic contrast for soft tissues, but also quantitative biochemical evaluation. Ultrashort time to echo (UTE) sequence, in particular, enables novel morphologic and quantitative evaluation of previously unseen MSK tissues. By using short minimum echo times (TE) below 1 msec, the UTE sequence can unveil short T2 properties of tissues including the deepest layers of the articular cartilage, cartilaginous endplate at the discovertebral junction, the meniscus, and the cortical bone. This article will discuss the application of UTE to evaluate these MSK tissues, starting with tissue structure, MR imaging appearance on standard versus short and ultrashort TE sequences, and provide the range of quantitative MR values found in literature.

Keywords: Articular cartilage; cortical bone; meniscus; ultrashort time to echo (UTE); cartilaginous endplate; discovertebral junction

Submitted Nov 03, 2016. Accepted for publication Dec 05, 2016.
doi: 10.21037/qims.2016.12.06
View this article at: http://dx.doi.org/10.21037/qims.2016.12.06

Introduction

Imaging investigation of the musculoskeletal (MSK) system has undergone substantial evolution in the last century. Advances in medical technology over the last decades have emphasized non-invasive evaluation of MSK tissues for diagnosis, characterization and response to therapy. Historically, the primary strength of magnetic resonance imaging (MRI) was its superior soft tissue contrast, while its performance lagged behind X-ray, computed tomography (CT) and ultrasound (US) in considerations of resolution. More recently, through radiofrequency (RF) coil and pulse sequence development, MRI rivals other imaging methods in this regard. Tissue contrast and adequate resolution provide the basis for morphologic evaluation, indicating whether structural integrity is preserved. Not only has hardware and software development in MRI focused on optimizing morphologic evaluation of tissue, it has segued into biochemical evaluation with quantitative methods that actually reflect the biochemical composition of MSK tissues. This proved to be a paradigm shift in non-invasive evaluation of MSK tissues as it provided objective data in the form of quantitative measures that could be followed over time.

Biomarker is a term defined by the National Institutes of Health Biomarkers Definitions Working Group in 1998 (1), and referred to a characteristic that is objectively measured and evaluated as an indicator of normal biological processes, pathogenic processes, or pharmacologic responses to a therapeutic intervention. Biomarker can be anything from a pulse measurement to any test of blood or tissue. In the other words, biomarker can be any sign that can be objectively measured in a reproducible fashion. Given the aforementioned advances in MSK MRI, coupled with the added advantages of no ionizing radiation, data acquisition

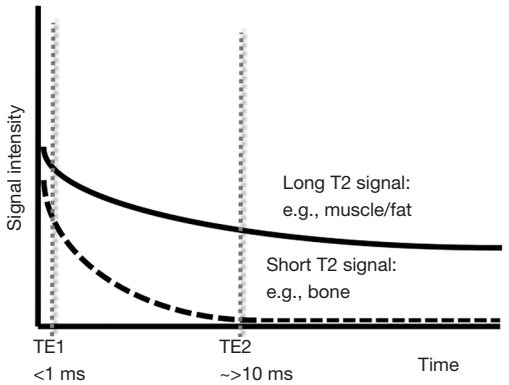

Figure 1 A graph of T2 decay comparing short and long T2 tissues. At TE longer than 10 msec the short T2 signal demonstrates complete relaxation. At TE less than 1 msec, both short and long T2 components contribute to the signal.

that lends itself to reproducible morphologic and quantitative assessment, and its intrinsically non-invasive nature, MRI is the imaging method that has emerged with valuable biomarkers for the MSK system. Historically these biomarkers have focused on the biochemical building blocks that predominate in most MSK tissues, collagen and proteoglycan. Very broadly, MR measurements that reflect the state of collagen (T2 measurements) and proteoglycan (delayed Gadolinium Enhanced MRI of Cartilage (dGEMRIC), T1 rho, sodium imaging, etc.) have been proposed in the literature, albeit few implemented broadly in clinical practice. A body of literature has emphasized that many MSK tissues are predominantly short T2 in nature, rendering them anechoic and that pulse sequences that allow signal to be acquired from these tissues affords qualitative assessment of morphology and quantitative biomarker assessment that is more sensitive than standard pulse sequences.

This manuscript will focus on application of short echo time (TE) and ultrashort echo time (UTE) MR imaging sequences to evaluate MSK tissues. It will review tissue structure, MR imaging appearance on standard versus short TE sequences, and emphasize a range of T2* values that can be expected in these tissues. In so doing, it provides a foundation for consideration of more detailed technical development or clinical application.

MR tissue property and UTE technique

Classic diagnostic considerations in conventional MR have focused primarily on tissue morphology and signal intensity characteristics. Tissue signal intensity reflects tissue property, broadly resulting from proton interactions between proteins and water, as well as the behavior of those protons based upon degree of binding. For example, tightly bounded water and proton in protein results in much shorter T2 tissue behavior than free water. From a clinical standpoint, it can be useful to divide MSK tissues into two general groups; those with majority of short T2 components and those representing longer T2 tissues. There is an abundance of short T2 tissues in the MSK system, including cortical bone, tendon, ligament, calcified cartilage, fibrocartilage (meniscus, labrum), and vertebral endplate. These tissues demonstrate signal void on all conventional MR sequences. The usual range of prescribed TE values for conventional sequences ranges from 10–80 msec. Because of the tissue structure, it demonstrates faster transverse magnetization decay. At the time of signal acquisition, the signal of these structures has undergone full relaxation resulting in signal void on conventional pulse sequences. In order to acquire signal intensity from these tissues shorter TE times must be applied (*Figure 1*).

The broad and general characterization of short versus long T2 tissues is clearly a crude way to acquire a basic understanding of tissue behavior. Robson *et al.* (2) approached tissue property from the standpoint of dipolar interaction between immobile nuclei. In this case, the more solid the material, the more short T2 properties would be expressed. While tendon and ligament are soft tissue structures, their biochemical composition and infrastructure (collagen fiber orientation and interaction with water molecules) dictate its MR properties and susceptibility to effects such as "magic angle." This is the case for each MSK tissue and emphasizes the necessity to tailor MR protocols (both qualitative and quantitative) to the known MR properties of those tissues (*Table 1*).

With regard to non-invasive characterization of MSK tissue, consideration of the effect of pathologic conditions must also be addressed. Variable types of pathology will clearly manifest in different ways. Increases in interstitial fluid, as with tendon or ligament tear, inflammation, mucoid transformation among other processes, would introduce long T2 elements within predominantly short T2 tissues. On the contrary, cellular infiltration such as fibrosis, iron deposition, amyloidosis and some stages of calcification or hemorrhage would manifest with short T2 properties.

Using ultrashort echo time (UTE) sequences, the TE can be decreased to below 1 msec in order to

Table 1 Published T2 values of MSK tissues with short T2 properties

Musculoskeletal tissue	Approximate T2 property (msec)	References
Temporomandibular disc	22.4–28.8	(3)
Meniscus	11.4±3.9	(4)
Cartilage of patella	32.1–35.0	(5)
Cartilage end plate	2.9	(6)
Zone of calcified cartilage patellar	2.0	(7)
Achilles tendon	1.1–1.7	(8,9)
Wet cortical bone (bicomponent analysis)	0.30 (85.2%) 2.29 (14.8%)	(10)
Dry cortical bone	0.22	(10)

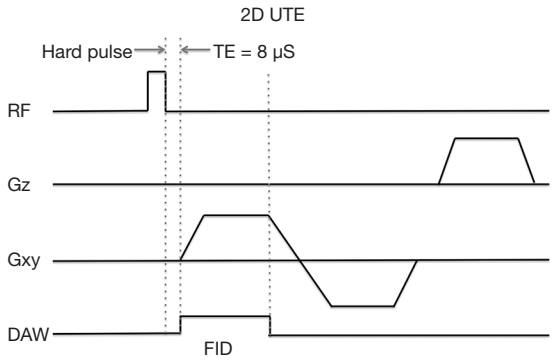

Figure 2 2D UTE diagram. Half pulse RF stimulation followed by rapid acquisition can reduce TE down to as low as 8 μsec.

acquire signal from the short T2 components in tissues. Historically, both hardware (fast transmit-receive switch) and software developments were implemented to decrease TE. Half width RF pulses were used, followed closely by slice selection gradients with projection reconstruction facilitating early collection of data during half of the excitation pulse. Data from two half excitations were subsequently combined to fill a single radial line of the k-space (6). This allowed 2D UTE sequences to have TE values 10–20 times shorter than conventional sequences (*Figure 2*). A technical limitation with the radial acquisition was the need for multiple acquisitions to fulfill the Nyquist criteria in comparison to Cartesian sampling, making sequence duration prohibitive. This has been addressed in varying ways to allow adequate coverage of the k-space.

The UTE sequence has extended MR evaluation of MSK tissues by allowing signal to be acquired from short T2 tissues, affording visual assessment of tissue infrastructure. Further, a large body of literature supports the hypothesis that quantitative MR evaluation of short T2 tissues, in the setting of early stages of disease with mild structural alteration, may be more sensitive than techniques designed for long T2 tissues (11,12). In an ideal setting, the imaging protocol would be tailored to the MR property of each specific tissue. T2 and T2* relaxation times can be measured by using a constant TR-multiple TE technique. As a general rule, TE values on both sides of the normal T2/T2* of the tissue in question would comprise data acquisition points for the decay curve. Signal intensity (SI) is measured in a region of interest (ROI) at each TE and plotted against it, resulting in a decay curve. Curve fitting can be mono-exponential or through bicomponent analysis. Quantitative data is often displayed through the use of color maps.

While there are clear advances made possible by UTE MR imaging in MSK systems, there are several shortcomings that could be overcome before a widespread clinical utilization is achieved. UTE obtains signal from tissues with short and long tissues, and lacks appropriate image contrast to replace conventional diagnostic sequences for evaluation of long T2 tissues. As such, UTE imaging may be performed in addition to clinical sequences, which increases overall time and cost. For short T2 evaluation, it has yet to be established how best to achieve short T2 contrast. While there are mounting evidence for the utility of UTE, one hurdle is the current lack of availability of UTE sequence in many vendor platforms, as well as additional cost when it becomes available.

Calcified layer articular cartilage

Structure

The articular cartilage is a connective tissue composed primarily of Type II collagen and proteoglycan, organized into a complex extracellular matrix designed to absorb shock during joint loading. The majority of articular cartilage MR literature has historically focused upon morphologic evaluation of the tissue. In the past years, biochemical evaluation in the form of quantitative assessment has emphasized the zonal configuration of the tissue with matrix organizational differences in deep versus superficial layers. Little attention has been afforded to the deepest layer of articular cartilage, that of the calcified cartilage layer (100–200 μm thick, Type X collagen), as classic MR contrast

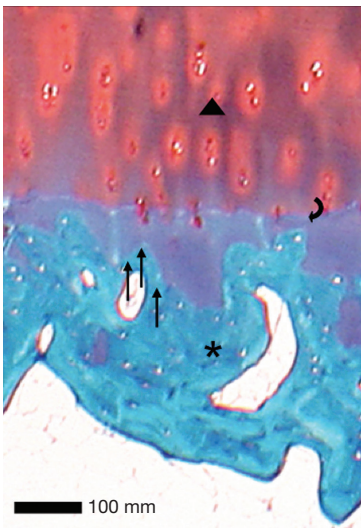

Figure 3 Hematoxylin and eosin stained histology of cartilage showing layer of superficial hyaline cartilage (triangle), tide mark (curve arrow), and calcified cartilage (asterisk) with interdigitation (arrow) into the subchondral bone (square).

mechanisms did not allow visualization of this structure (7,13,14). Histologically, the calcified cartilage is shown to interdigitate into the subchondral bone plate, allowing it to anchor the more superficial cartilage to bone and to establish the osteochondral junction (6) (*Figure 3*).

Function and importance

The calcified cartilage and subchondral bone plate play a vital role in creating a transition from ossified to non-ossified tissue that dissipates stress and facilitates a more robust biomechanical environment. This region is also vital to the nutritional and vascular health of the osteochondral junction as it accommodates its primary vascular supply (15).

For these reasons, the osteochondral junction, and more specifically, the calcified layer of cartilage, has been implicated in one theory of osteoarthritis (OA) pathogenesis. This theory suggests that degenerative joint changes emanate from the bone/osteochondral junction rather than from superficial cartilage lesions. Failure of the calcified layer can manifest as both thinning, postulated to represent an earlier phase in the process of degeneration, and ultimately thickening due to angiogenesis related to bone turnover and remodeling (15). The latter includes duplication of the tidemark, resulting in thinning of superficial cartilage. Further, thickening of the subchondral bone plate also occurs. Although the bone volume is increased, the bone mineralization is reduced with a marked decrease calcium-to-collagen ratio. The thinning of the overlying non-calcified cartilage and stiffened subchondral bone plate makes the structure more susceptible to damage from shearing force and ultimate degeneration (16).

The role of the calcified layer of cartilage has also been emphasized in the setting of cartilage repair, specifically in the microfracture technique. With this technique, chondral lesions are debrided, with recent literature advocating removal of the native calcified cartilage (17). The subchondral bone plate is fenestrated to allow pluripotent stem cell migration into the defect, and ultimately formation of a fibrocartilaginous fill tissue. For this procedure to be successful, repaired tissue must form and it must adhere to the bone through reconstitution of the calcified layer of cartilage. Without adherence, the repair tissue can delaminate from the underlying bone.

MR imaging

Given the structural, functional and clinical importance of the calcified layer of cartilage, it is clear that a non-invasive means of evaluation of this tissue would be valuable. The T2* of the calcified layer of cartilage is on the order of 1 msec, hence its designation as a short T2 tissue, and therefore, one that has historically been 'invisible' on standard MR pulse sequences. In a landmark paper by Bae *et al*., the normal appearance of the calcified layer was established as a well-defined linear region of high signal intensity at the junction of superficial cartilage and subchondral bone (18) (*Figure 4*).

In order to optimize contrast and visualization of the calcified cartilage, a subtraction technique and double adiabatic inversion recovery (DIR) pulse sequence, among others, have been described (19,20). The subtraction technique involves a two echo acquisition whereby the longer TE (6.6 msec) acquisition is subtracted from the shorter TE (0.008 msec) acquisition, resulting in primarily ultrashort T2 signal in the image. The calcified cartilage layer becomes bright and easily visible compared to the adjacent cartilage and subchondral bone. The DIR technique implements an adiabatic inversion pulse to null the fat and longer T2 tissue signal (including water), thereby unmasking the signal from the deepest calcified layer of cartilage (7).

Morphologically, the calcified cartilage could be thin,

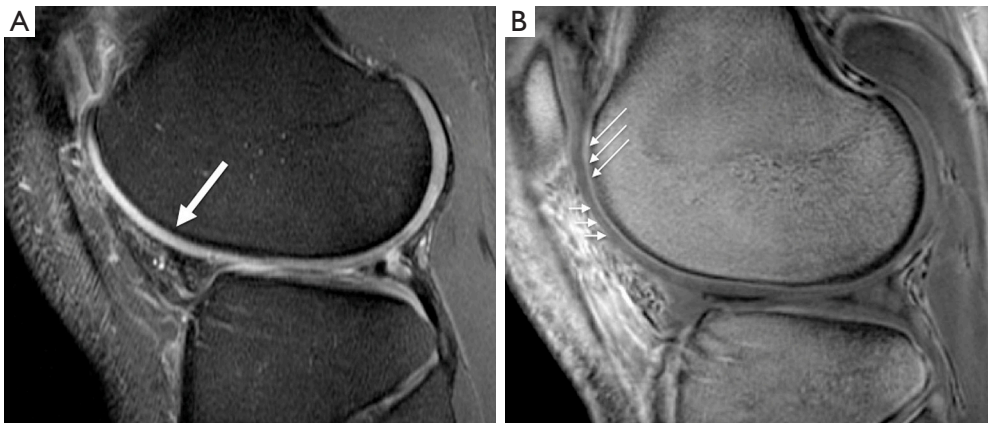

Figure 4 Sagittal MR images of the knee. (A) PDFS (TE =50 msec) demonstrates intermediate signal intensity of the superficial articular cartilage and low intensity of the deep layer; (B) UTE T2* (TE =8 μsec) reveals high intensity of the calcified cartilage layer (long thin arrow) and intermediate signal intensity of the uncalcified cartilage (short thin arrow).

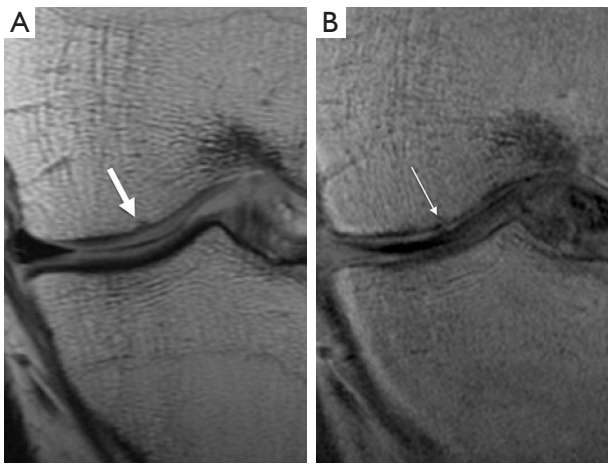

Figure 5 Coronal MR images of the knee. (A) PD (TE =55 msec) shows focal sclerosis of the subchondral bone with intact articular cartilage surface (thick arrow); (B) subtracted UTE T2* image (TE 8 μsec–TE 6 msec) demonstrates a tiny focal defect of the calcified cartilage layer overlying the region of subchondral bone sclerosis.

thick and ill-defined, or absent correlating with the histologic findings seen in degeneration as well as acute injury (*Figure 5*). A recent article by Hargrave-Thomas *et al*., showed increased calcified layer thickness with increasing grades of degeneration (21). The authors concluded that the mechanical transition from calcified cartilage to subchondral bone involves a graded continuum of increasing material stiffness that is altered with degeneration and reflected by the thickened calcified cartilage layer.

Quantitative assessment

The T2 value of the articular cartilage is about 32.1–35.0 msec (5) while that of the calcified cartilage is as short as 1.0–3.3 msec (7). Generally, T2* is calculated in the calcified layer of cartilage with a mono- or bi-exponential decay model (22). Several reports establish an increased T2* in the setting of calcified layer cartilage degeneration (5,23,24). Williams, *et al*., showed UTE T2* mapping of the cartilage end plate (CEP) to be more sensitive to collagen matrix disorganization/degeneration than standard T2 values using polarized microscopy as a reference standard (11). Further, bi-component analysis of CEP by Pauli *et al*., found the short T2* water fraction correlates significantly with histopathological scores in cartilage degeneration (25). Chu *et al*. found UTE T2* to be useful in evaluation and follow up of cartilage in post anterior cruciate ligament (ACL) reconstruction patients (26). The study revealed significantly increased T2* values in the calcified layer cartilage in an ACL injury group without visible superficial cartilage lesions on arthroscopic evaluation. In addition, longitudinal follow up T2* values significantly decreased during a 2-year period after ACL reconstruction. The result demonstrates the capability of the UTE sequence to demonstrate deep cartilage matrix change and suggests that the injury to the calcified layer is reversible (26). Such findings emphasize the importance of non-invasive MR evaluation in the setting of longitudinal follow-up of injury, as well as the potential of UTE MR to serve as a valuable biomarker for osteoarthritis.

Discovertebral junction

Structure

The intervertebral disc is comprised of three distinct tissues: annulus fibrosus (AF), nucleus pulposus (NP), and the cartilaginous endplate (CEP). The NP is described as a network of Type II collagen fibrils, embedded in a proteoglycan-rich gelatinous matrix. It is located within the center of the disc and surrounded by the AF, highly organized collagen-rich lamellae that transition from Type II collagen at the NP interface, to Type I collagen in its periphery (27). The CEP is a thin layer of hyaline cartilage (approximately 600 μm) that resides between the intervertebral disc and the bony vertebral endplate (VEP). It is rich in Type II collagen and proteoglycan (28). Similar to the articular cartilage in the knee, the CEP also has a deep calcified portion in which vascular canals are located, and similar to this tissue in the knee, it is comprised of Type X collagen (27). The CEP thickness does not appear to vary throughout the lumbar spine, but has been shown to be thinner toward the center of the disc, referred to as a V-shaped pattern along the anterior-posterior disc axis (29,30). Studies have also characterized the cartilaginous endplate axial area, anterior-posterior width and lateral width for the purposes of analyzing its overall geometry (30).

Function and importance

The CEP plays an important role in mechanical stability of the disc, as well as nutrient transport. Some literature suggests that the CEP may regulate disc matrix degradation through molecular interactions (31).

Biomechanically, the CEP plays a crucial role in transferring mechanical loads between the intervertebral disc and bone. The annulus fibrosis is loaded largely in tension while the swelling pressure of the nucleus pulposus resists compression between the vertebral bodies (32). The mismatch of stiff bone and relatively soft cartilage at the discovertebral junction transitions through the calcified CEP as it provides a successful interface with bone and cartilage reflected by low incidences of in vivo failure (33).

Two distinct routes of nutrient transport have been proposed, (I) into the intervertebral disc via the CEP and (II) via the annulus fibrosis periphery (34). The majority of the disc relies on the endplate route. Capillaries penetrate channels in the subchondral bone plate and terminate in loops at the discovertebral junction. The density and integrity of the capillary beds diminish with age (35,36). Further, architectural changes in the capillary bed or porosity of the CEP have important consequences for delivery of nutrients to the disc, which in turn lead to degenerative changes in the disc as well as the vertebral body (37,38).

Recent work has focused on acute loading patterns in the spine, and shown annulus-endplate junction discontinuity as the failure pattern when acute rapid rate compression is introduced to the spine. This work suggests that foci of annulus-endplate failure precede frank external herniation of the disc depending on the location of the initial insult (39). Conversely, it appears complex, chronic repetitive loading patterns (lower force compression, lower rate of introduction) may fail at the end plate junction, but leave the cartilaginous endplate intact and without immediate external disc herniation (40). Both cases, disc herniation and architectural distortion of the CEP, can lead to more long term degenerative changes at the disc-end plate junction.

Structural changes in the CEP and its calcified cartilage have been implicated in disc degeneration. Thinning of the CEP and thickening of its calcified cartilage have been postulated to inhibit passage of nutrients to the disc (41). The ultimate end path is loss of intervertebral disc architecture with disc space narrowing as well as reactive changes in the vertebral body.

Two basic components of the Schmorl's nodes are disruption of the endplate and herniation of the nucleus pulposus. The Schmorl's nodes have an uncertain etiology, some appear to be more clinically significant than others. The Schmorl's nodes can be accidentally found on MR images without symptoms (around 10%), though there appears to be a statistically significantly higher rate in back pain patients (42). Most congenital Schmorl's nodes are asymptomatic, while traumatic or degenerative Schmorl's nodes are more likely to correlate with back pain (43). Vascularized Schmorl's node with adjacent marrow edema has a higher association with back pain. The VEP lesion can contribute to biomechanical weakening and thinning of the CEP (44).

MRI appearance

On standard MR evaluation, fast spin echo (FSE) T2-weighted images are generally implemented to evaluate the intervertebral disc and discovertebral junction. With early degenerative disc disease, there is a loss of signal intensity within the nucleus pulposus. Degenerative changes progress with disc herniation, loss of intervertebral disc space height

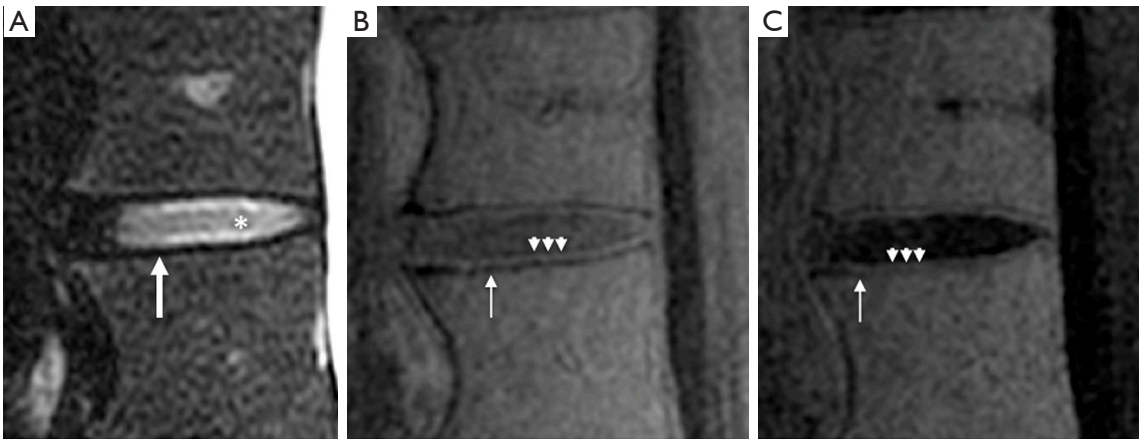

Figure 6 Sagittal MR image of L1/2 level (A) T2 fat saturated (TE = 75 msec) reveals high signal intensity of the nucleus pulposus (asterisk) and marked low signal intensity of the CEP and VEP (thick arrow); (B) UTE T2* (TE = 8 µsec) and (C) Subtraction UTE T2* (TE 8 µsec – TE 2.8 msec) shows intermediate to high signal intensity of the CEP (arrowheads) and low signal intensity of the VEP (thin arrow).

Figure 7 Sagittal UTE subtraction image of the cadaveric spine (TE 8 µsec–TE 10 msec) reveals multiple Schmorl's nodes (arrows). Thinning and irregularity of the cartilaginous end plate at the site of Schmorl's nodes are observed.

and altered morphology and signal within the vertebral body (i.e., Modic change). Evaluation of the CEP and VEP are suboptimal on conventional MR sequences as both are short T2 tissues and appear anechoic on standard MR pulse sequences.

The UTE sequence affords a contrast mechanism to allow visualization of the CEP, as validated by histologic correlation by Bae *et al*. (16). The CEP on UTE MR sequences has a bilaminar linear intermediate to high signal appearance with a thicker superficial and a thinner deep layer consistent with non-calcified cartilage and calcified cartilage layers respectively (*Figure 6*).

Several recent in vivo studies demonstrate good correlation between abnormal CEP morphology seen on UTE MRI and vertebral end plate lesions (45). Abnormal morphology of the CEP can be demonstrated by signal loss, thinning, thickening and irregularity (*Figure* 7). Thinning and absence of the CEP has been noted on histology in aging human donor tissue (35). Thickening of the CEP may be due to increase vascularity of the end plate, resulting in overgrowth of the tidemark as in the knee. Calcium deposition at the CEP may cause an irregular appearance. In Schmorl's nodes the structural alteration of VEP and CEP have a strong correlation, though the CEP lesion can be variable (17).

Precise MR quantification of the osteochondral junction is difficult due to the fact the structure is so thin. Several studies have addressed the T2* relaxation of CEP. Bae *et al*., found the T2* value of the CEP to be around 3 msec (6). Another cadaveric study by Aaron, *et al*., found T2 relaxation times on the order of 9.9 msec with a trend to closer to the VEP (46). These studies further documented that MR may serve as a biomarker in the CEP.

Meniscus

Structure

The menisci are fibrocartilaginous, C-shaped wedge

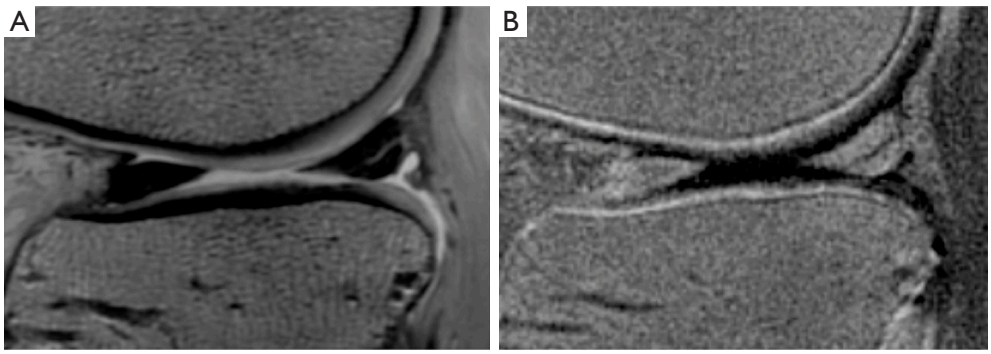

Figure 8 Sagittal images of medial meniscus. (A) PD image (TE = 40 msec) reveals a subtle band of high signal intensity at the posterior horn of the medial meniscus without definite surface extension; (B) subtracted UTE T2* (TE 8 μsec – TE 4 msec) shows a hypo-intense band at the posterior horn of the medial meniscus with surface extension suspicious of tear.

structures interposed between the femoral and tibial articular surfaces of the knee that facilitate even distribution of weight bearing forces across the tibial plateau. They are primarily comprised of collagen (60–70%), with some proteoglycan (2–8%) (47). A complex collagen (Type I) fibrillar network dominated by the circumferential and radial fiber groups provides a mesh-like infrastructure for this tissue (48-50). The menisci are relatively avascular, with only the peripheral 10–25% receiving perforating vascular channels from the adherent synovial lining (51). The menisci have osseous attachments at the anterior and posterior horns of both the medial and lateral menisci, referred to as root ligaments.

Function and importance

The menisci are vital structures in the joint health of the knee and have many roles. They facilitate joint congruity, distribute load across the joint, assist in joint lubrication, provide shock-absorption, and aid in joint proprioception (52-56). Once these functions are impaired, there is increased risk of degeneration with an emerging clinical and scientific body of evidence that suggests meniscal deficiency predisposes to early osteoarthritis (57). Removal of the meniscus has been shown to increase peak contact stress in the affected compartment, resulting in significant chondral loss (58,59). Further, increases in contact stress have been shown to be directly proportional to the amount of meniscus removed (60). On the contrary, restoration of partial lesions has been shown to approximate contact mechanics, emphasizing the overarching theme that the goal of meniscal treatment is to preserve form and therefore function (61).

MR imaging

The meniscus, seen on conventional MR, is homogeneously low in signal intensity due to its short T2 properties. Meniscal failure is classically distinguished as traumatic versus degenerative. Historical meniscal classification schemes distinguished intrasubstance degenerative change from tear (traumatic or degenerative) with tears characterized by linear signal that extended to a joint surface of the meniscus (62) (*Figure 8*). Conventional MRI can demonstrate meniscal tears with high sensitivity and specificity (80–90% and 95–97%, respectively) (34) as compared to arthroscopy. The intermediate TE sequences, such as proton density, have more favorable diagnostic potential as compared to longer TE sequences. This is proposed to be due to the fact that the water molecules within the tear are bound water rather than free water. However, in diagnosis of root tear, the T2 with fat suppression technique has higher accuracy (37) (*Figure 9*).

Due to the ability to acquire signal from short T2 tissues, UTE sequences can unmask the collagen fibrillar infrastructure of the meniscus. At TE times below 1 msec, the meniscus demonstrates uniform bright signal intensity. At TE times 3-6 msec, the contrast within the meniscus appears optimal for visualization of the collagen fibrillar network. Meniscal calcifications have also been characterized with UTE sequences.

Quantitative assessment

Quantitative analysis of the meniscus has been performed using a constant TR, variable TE technique with TE values ranging from 0.008 to 40 msec. Mean T2* relaxation times

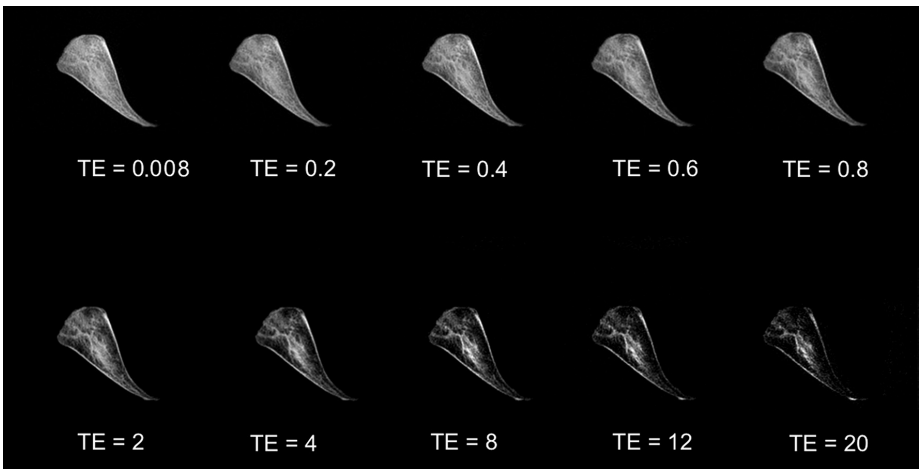

Figure 9 UTE of cadaveric menisci at different TE values: 0.008, 0.2, 0.4, 0.6, 0.8, 2, 4, 8, 12, and 20 msec. The image reveals the infrastructure of the meniscus. The image obtained at TE of 4 msec provides the best contrast in evaluation of the infrastructure.

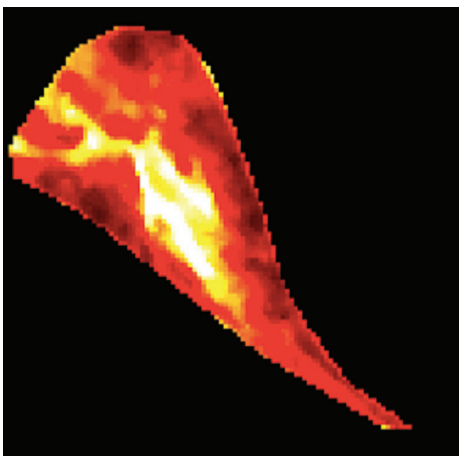

Figure 10 T2 mapping of menisci demonstrating spatial distribution of the T2 relaxation time.

of the normal meniscus have been reported in the 4–10 msec range. It appears that increased T2* values may indicate subclinical meniscal degeneration (63). Williams *et al*., has found heterogeneous of the T2*map are suggestive of collagen disorganization introducing the potential for identification of focal structural change within the meniscus (64) (*Figure 10*).

Cortical bone

Structure

Cortical bone comprises the bulk of the adult skeletal mass (approximately 80%) with an internal system of pores (Haversian canals, Volkmann's canals, resorption cavities, lacuna and canaliculi) that accommodate blood vessels, nerves and osteocytes (47). It is composed of about 15% water by volume (bound to collagen or free, residing within spaces), and 85% Type I collagen and calcium hydroxyapatite (65). Its thickness ranges from 1 to 5 mm and varies with changes in specific bone morphology. In general, bone is a dynamic tissue engaged in a constant equilibrium between formation (osteoblast activity) and resorption (osteoclast activity). Dynamic equilibrium and structural remodeling is governed by many factors, among them mechanical demands and hormonal regulation.

Function and importance

There are many functions of bone, among them to facilitate locomotion, serve as a protective shell for the internal organs, and to serve as a depot for the body's calcium requirements. Broadly speaking, bone can fail through a variety of mechanisms. Healthy bone can be exposed to acute trauma that may exceed its material property resulting in fracture. In the setting of chronic repetitive microtrauma, the traumatic insult may exceed the ability of the bone to repair, and result in a spectrum of failure from incomplete to complete fracture. Decreased quantity and quality of bone, in osteoporosis or as mitigated through alterations in mechanical stimulation or hormonal variation, are also factors that can ultimately affect bone strength and result in

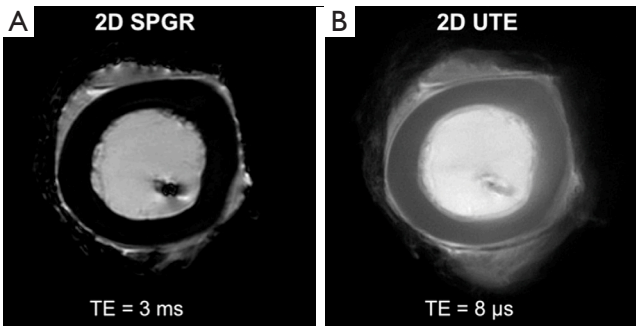

Figure 11 Axial MR imaging of a bovine bone at mid-tibia. (A) Spoiled gradient echo and (B) UTE MR images. Higher signal intensity of the cortical bone is seen on UTE sequence. Image courtesy of Dr. Jiang Du.

failure in the form of fracture. Clearly processes that affect quantity and quality of bone may also have ramifications for calcium metabolism that could affect the entire body.

MR imaging

Normal adult cortical bone has a very short T2 and characteristically produces no signal with pulse sequence echo times used in clinical MRI protocols. Three pools of protons have been identified in cortical bone using spectroscopic evaluation. These include collagen methylene protons, collagen-bound water, and a broad peak consisting of pore water and lipid (66). UTE sequences have been successful at acquiring signal from cortical bone.

Quantitative assessment

Mono-exponential T2* values for cortical bone are reported in the 0.39–0.5 msec range (67,68). With quantitative assessment of cortical bone, measuring the bound water versus free water appears to allow characterization of organic matrix versus cortical porosity. This can be achieved through several clinically compatible techniques. These include bicomponent analysis, single adiabatic inversion or double adiabatic inversion (69). More recently, the UTE-derived indices of porosity index and suppression ratio have been described and show potential for clinical implementation (70,71). Some literature suggests that quantitative assessment of cortical bone may be correlated with material property of the tissue. Bae *et al.*, found positive correlation between failure strain of the cadaveric femoral bone and short T2 relaxation time. Negative correlation was found between ultimate stress and total water as well as bounded water content. These are promising results that present a novel method to evaluate cortical bone quality, as well as quantity, in a non-invasive manner (72) (*Figure 11*).

Conclusions

In conclusion, UTE MR sequences offer a paradigm shift in the non-invasive evaluation of many MSK tissues, offering a contrast mechanism that can be exploited to evaluate tissue infrastructure before severe alteration occurs. Clearly, this tool will be valuable in diagnosis and characterization of tissues, with promise to serve as both a structural and functional surrogate.

Acknowledgements

Funding: This article was made possible in party by grants from the Clinical Science Research & Development of the Veterans Affairs Office of Research and Development (Award Number 5I01CX000625; Project ID: 1161961) in support of Dr. Christine B. Chung, and the National Institute of Arthritis and Musculoskeletal and Skin Diseases (NIAMS) of the National Institute of Health (NIH) in support of Dr. Christine Chung (Grant Number R01 AR064321) and in support of Dr. Won C. Bae (Grant Number R01 AR066622).

Footnote

Conflicts of Interest: The authors have no conflicts of interest to declare.

Disclaimer: The contents of this paper are solely the responsibility of the authors and do not necessarily represent the official views of the funding agencies.

References

1. Strimbu K, Tavel JA. What are biomarkers? Curr Opin HIV AIDS 2010;5:463-6.
2. Robson MD, Gatehouse PD, Bydder M, Bydder GM. Magnetic resonance: an introduction to ultrashort TE (UTE) imaging. J Comput Assist Tomogr 2003;27:825-46.
3. Schmid-Schwap M, Bristela M, Pittschieler E, Skolka A, Szomolanyi P, Weber M, Piehslinger E, Trattnig S. Biochemical analysis of the articular disc of the

temporomandibular joint with magnetic resonance T2 mapping: a feasibility study. Clin Oral Investig 2014;18:1865-71.
4. Rauscher I, Stahl R, Cheng J, Li X, Huber MB, Luke A, Majumdar S, Link TM. Meniscal measurements of T1rho and T2 at MR imaging in healthy subjects and patients with osteoarthritis. Radiology 2008;249:591-600.
5. Dunn TC, Lu Y, Jin H, Ries MD, Majumdar S. T2 relaxation time of cartilage at MR imaging: comparison with severity of knee osteoarthritis. Radiology 2004;232:592-8.
6. Bae WC, Biswas R, Chen K, Chang EY, Chung CB. UTE MRI of the Osteochondral Junction. Curr Radiol Rep 2014;2:35.
7. Du J, Carl M, Bae WC, Statum S, Chang EY, Bydder GM, Chung CB. Dual inversion recovery ultrashort echo time (DIR-UTE) imaging and quantification of the zone of calcified cartilage (ZCC). Osteoarthritis Cartilage 2013;21:77-85.
8. Gärdin A, Rasinski P, Berglund J, Shalabi A, Schulte H, Brismar TB. T2 * relaxation time in Achilles tendinosis and controls and its correlation with clinical score. J Magn Reson Imaging 2016;43:1417-22.
9. Grosse U, Springer F, Hein T, Grözinger G, Schabel C, Martirosian P, Schick F, Syha R. Influence of physical activity on T1 and T2* relaxation times of healthy Achilles tendons at 3T. J Magn Reson Imaging 2015;41:193-201.
10. Biswas R, Bae W, Diaz E, Masuda K, Chung CB, Bydder GM, Du J. Ultrashort echo time (UTE) imaging with bi-component analysis: bound and free water evaluation of bovine cortical bone subject to sequential drying. Bone 2012;50:749-55.
11. Williams A, Qian Y, Bear D, Chu CR. Assessing degeneration of human articular cartilage with ultra-short echo time (UTE) T2* mapping. Osteoarthritis Cartilage 2010;18:539-46.
12. Bae WC, Statum S, Zhang Z, Yamaguchi T, Wolfson T, Gamst AC, Du J, Bydder GM, Masuda K, Chung CB. Morphology of the cartilaginous endplates in human intervertebral disks with ultrashort echo time MR imaging. Radiology 2013;266:564-74.
13. Bae WC, Dwek JR, Znamirowski R, Statum SM, Hermida JC, D'Lima DD, Sah RL, Du J, Chung CB. Ultrashort echo time MR imaging of osteochondral junction of the knee at 3 T: identification of anatomic structures contributing to signal intensity. Radiology 2010;254:837-45.
14. Lane LB, Bullough PG. Age-related changes in the thickness of the calcified zone and the number of tidemarks in adult human articular cartilage. J Bone Joint Surg Br 1980;62:372-5.
15. Li G, Yin J, Gao J, Cheng TS, Pavlos NJ, Zhang C, Zheng MH. Subchondral bone in osteoarthritis: insight into risk factors and microstructural changes. Arthritis Res Ther 2013;15:223.
16. Goldring SR. Role of bone in osteoarthritis pathogenesis. Med Clin North Am 2009;93:25-35, xv.
17. Frisbie DD, Morisset S, Ho CP, Rodkey WG, Steadman JR, McIlwraith CW. Effects of calcified cartilage on healing of chondral defects treated with microfracture in horses. Am J Sports Med 2006;34:1824-31.
18. Bae WC, Tafur M, Chang EY, Du J, Biswas R, Kwack KS, Healey R, Statum S, Chung CB. High-resolution morphologic and ultrashort time-to-echo quantitative magnetic resonance imaging of the temporomandibular joint. Skeletal Radiol 2016;45:383-91.
19. Du J, Takahashi AM, Bae WC, Chung CB, Bydder GM. Dual inversion recovery, ultrashort echo time (DIR UTE) imaging: creating high contrast for short-T(2) species. Magn Reson Med 2010;63:447-55.
20. Du J, Bydder M, Takahashi AM, Carl M, Chung CB, Bydder GM. Short T2 contrast with three-dimensional ultrashort echo time imaging. Magn Reson Imaging 2011;29:470-82.
21. Hargrave-Thomas E, van Sloun F, Dickinson M, Broom N, Thambyah A. Multi-scalar mechanical testing of the calcified cartilage and subchondral bone comparing healthy vs early degenerative states. Osteoarthritis Cartilage 2015;23:1755-62.
22. Qian Y, Williams AA, Chu CR, Boada FE. Multicomponent T2* mapping of knee cartilage: technical feasibility ex vivo. Magn Reson Med 2010;64:1426-31.
23. Prasad AP, Nardo L, Schooler J, Joseph GB, Link TM. T(1) rho and T(2) relaxation times predict progression of knee osteoarthritis. Osteoarthritis Cartilage 2013;21:69-76.
24. Friedrich KM, Shepard T, de Oliveira VS, Wang L, Babb JS, Schweitzer M, Regatte R. T2 measurements of cartilage in osteoarthritis patients with meniscal tears. AJR Am J Roentgenol 2009;193:W411-5.
25. Pauli C, Bae WC, Lee M, Lotz M, Bydder GM, D'Lima DL, Chung CB, Du J. Ultrashort-echo time MR imaging of the patella with bicomponent analysis: correlation with histopathologic and polarized light microscopic findings. Radiology 2012;264:484-93.
26. Chu CR, Williams AA, West RV, Qian Y, Fu FH, Do BH, Bruno S. Quantitative Magnetic Resonance

Imaging UTE-T2* Mapping of Cartilage and Meniscus Healing After Anatomic Anterior Cruciate Ligament Reconstruction. Am J Sports Med 2014;42:1847-56.
27. Nosikova YS SJ, Grynpas M, Gibson G, Kandel RA. Characterization of the annulus fibrosus-vertebral body interface: identification of new structural features. J Anat 2012;221:577-89.
28. Schollmeier G L-ER, Lewandrowski KU. Observations on fiber-forming collagens in the anulus fibrosus. Spine (Phila Pa 1976) 2000;1;25:2736-41.
29. Moon SM, Yoder JH, Wright AC, Smith LJ, Vresilovic EJ, Elliott DM. Evaluation of intervertebral disc cartilaginous endplate structure using magnetic resonance imaging. Eur Spine J 2013;22:1820-8.
30. DeLucca JF, Peloquin JM, Smith LJ, Wright AC, Vresilovic EJ, Elliott DM. MRI quantification of human spine cartilage endplate geometry: Comparison with age, degeneration, level, and disc geometry. J Orthop Res 2016;34:1410-7.
31. Neidlinger-Wilke C, Boldt A, Brochhausen C, Galbusera F, Carstens C, Copf F, Schultheiss M, Lazary A, Brayda-Bruno M, Ignatius A, Wilke HJ. Molecular interactions between human cartilaginous endplates and nucleus pulposus cells: a preliminary investigation. Spine (Phila Pa 1976) 2014;39:1355-64.
32. Paietta RC BE, Ferguson VL. Mineralization and collagen orientation throughout aging at the vertebral endplate in the human lumbar spine. J Struct Biol 2013;184:310-20.
33. Moore RJ. The vertebral endplate: disc degeneration, disc regeneration. Eur Spine J 2006;15:S333-7.
34. Urban JP, Smith S, Fairbank JC. Nutrition of the intervertebral disc. Spine (Phila Pa 1976) 2004;29:2700-9.
35. Bernick S, Cailliet R. Vertebral end-plate changes with aging of human vertebrae. Spine (Phila Pa 1976) 1982;7:97-102.
36. Donisch EW TW. The cartilage endplates of the human vertebral column (some considerations of postnatal development). Anat Rec 1971;169:705-16.
37. Moore RJ, Osti OL, Vernon-Roberts B, Fraser RD. Changes in endplate vascularity after an outer anulus tear in the sheep. Spine (Phila Pa 1976) 1992;17:874-8.
38. Ayotte DC, Ito K, Perren SM, Tepic S. Direction-dependent constriction flow in a poroelastic solid: the intervertebral disc valve. J Biomech Eng 2000;122:587-93.
39. Wade KR, Robertson PA, Thambyah A, Broom ND. "Surprise" Loading in Flexion Increases the Risk of Disc Herniation Due to Annulus-Endplate Junction Failure: A Mechanical and Microstructural Investigation. Spine (Phila Pa 1976) 2015;40:891-901.
40. Berger-Roscher N, Casaroli G, Rasche V, Villa T, Galbusera F, Wilke HJ. Influence of Complex Loading Conditions on Intervertebral Disc Failure. Spine (Phila Pa 1976) 2016. [Epub ahead of print].
41. Lee SW, Mathie AG, Jackson JE, Hughes SP. Investigation of vertebral "end plate sclerosis". Skeletal Radiol 2001;30:454-9.
42. Hamanishi C, Kawabata T, Yosii T, Tanaka S. Schmorl's nodes on magnetic resonance imaging. Their incidence and clinical relevance. Spine (Phila Pa 1976) 1994;19:450-3.
43. Peng B, Wu W, Hou S, Shang W, Wang X, Yang Y. The pathogenesis of Schmorl's nodes. J Bone Joint Surg Br 2003;85:879-82.
44. Stäbler A, Bellan M, Weiss M, Gärtner C, Brossmann J, Reiser MF. MR imaging of enhancing intraosseous disk herniation (Schmorl's nodes). AJR Am J Roentgenol 1997;168:933-8.
45. Chen KC, Tran B, Biswas R, Statum S, Masuda K, Chung CB, Bae WC. Evaluation of the disco-vertebral junction using ultrashort time-to-echo magnetic resonance imaging: inter-reader agreement and association with vertebral endplate lesions. Skeletal Radiol 2016;45:1249-56.
46. Fields AJ, Han M, Krug R, Lotz JC. Cartilaginous end plates: Quantitative MR imaging with very short echo times-orientation dependence and correlation with biochemical composition. Radiology 2015;274:482-9.
47. Chang EY, Du J, Chung CB. UTE imaging in the musculoskeletal system. J Magn Reson Imaging 2015;41:870-83
48. Petersen W, Tillmann B. Collagenous fibril texture of the human knee joint menisci. Anat Embryol (Berl) 1998;197:317-24.
49. Kambic HE, McDevitt CA. Spatial organization of types I and II collagen in the canine meniscus. J Orthop Res 2005;23:142-9.
50. Skaggs DL, Warden WH, Mow VC. Radial tie fibers influence the tensile properties of the bovine medial meniscus. J Orthop Res 1994;12:176-85.
51. Arnoczky SP, Warren RF. Microvasculature of the human meniscus. Am J Sports Med 1982;10:90-5.
52. Levy IM, Torzilli PA, Warren RF. The effect of medial meniscectomy on anterior-posterior motion of the knee. J Bone Joint Surg Am 1982;64:883-8.
53. Shoemaker SC, Markolf KL. The role of the meniscus in the anterior-posterior stability of the loaded anterior cruciate-deficient knee. Effects of partial versus total

excision. J Bone Joint Surg Am 1986;68:71-9.
54. Clark JM, Norman AG, Kääb MJ, Nötzli HP. The surface contour of articular cartilage in an intact, loaded joint. J Anat 1999;195:45-56.
55. Voloshin AS, Wosk J. Shock absorption of meniscectomized and painful knees: a comparative in vivo study. J Biomed Eng 1983;5:157-61
56. Zimny ML, Albright DJ, Dabezies E. Mechanoreceptors in the human medial meniscus. Acta Anat (Basel) 1988;133:35-40
57. Hutchinson ID, Moran CJ, Potter HG, Warren RF, Rodeo SA. Restoration of the meniscus: form and function. Am J Sports Med 2014;42:987-98
58. Kurosawa H, Fukubayashi T, Nakajima H. Load-bearing mode of the knee joint: physical behavior of the knee joint with or without menisci. Clin Orthop Relat Res 1980:283-90.
59. Wang YX, Griffith JF, Ahuja AT. Non-invasive MRI assessment of the articular cartilage in clinical studies and experimental settings. World J Radiol 2010;2:44-54.
60. Baratz ME, Fu FH, Mengato R. Meniscal tears: the effect of meniscectomy and of repair on intraarticular contact areas and stress in the human knee. A preliminary report. Am J Sports Med 1986;14:270-5.
61. Galley NK, Gleghorn JP, Rodeo S, Warren RF, Maher SA, Bonassar LJ. Frictional properties of the meniscus improve after scaffold-augmented repair of partial meniscectomy: a pilot study. Clin Orthop Relat Res 2011;469:2817-23.
62. Stoller DW, Martin C, Crues JV 3rd, Kaplan L, Mink JH. Meniscal tears: pathologic correlation with MR imaging. Radiology 1987;163:731-5.
63. Du J, Diaz E, Carl M, Bae W, Chung CB, Bydder GM. Ultrashort echo time imaging with bicomponent analysis. Magn Reson Med 2012;67:645-9.
64. Williams A, Qian Y, Golla S, Chu CR. UTE-T2 * mapping detects sub-clinical meniscus injury after anterior cruciate ligament tear. Osteoarthritis Cartilage 2012;20:486-94.
65. Wehrli FW, Song HK, Saha PK, Wright AC. Quantitative MRI for the assessment of bone structure and function. NMR Biomed 2006;19:731-64
66. Horch RA, Gochberg DF, Nyman JS, Does MD. Non-invasive predictors of human cortical bone mechanical properties: T(2)-discriminated H NMR compared with high resolution X-ray. PLoS One 2011;6:e16359.
67. Techawiboonwong A, Song HK, Leonard MB, Wehrli FW. Cortical bone water: in vivo quantification with ultrashort echo-time MR imaging. Radiology 2008;248:824-33.
68. Du J, Bydder GM. Qualitative and quantitative ultrashort-TE MRI of cortical bone. NMR Biomed 2013;26:489-506.
69. Horch RA, Gochberg DF, Nyman JS, Does MD. Clinically compatible MRI strategies for discriminating bound and pore water in cortical bone. Magn Reson Med 2012;68:1774-84.
70. Rajapakse CS, Bashoor-Zadeh M, Li C, Sun W, Wright AC, Wehrli FW. Volumetric Cortical Bone Porosity Assessment with MR Imaging: Validation and Clinical Feasibility. Radiology 2015;276:526-35.
71. Li C, Seifert AC, Rad HS, Bhagat YA, Rajapakse CS, Sun W, Benny Lam SC, Wehrli FW. Cortical Bone Water Concentration: Dependence of MR Imaging Measures on Age and Pore Volume Fraction. Radiology 2016;280:653.
72. Bae WC, Chen PC, Chung CB, Masuda K, D'Lima D, Du J. Quantitative ultrashort echo time (UTE) MRI of human cortical bone: correlation with porosity and biomechanical properties. J Bone Miner Res 2012;27:848-57.

Cite this article as: Siriwanarangsun P, Statum S, Biswas R, Bae WC, Chung CB. Ultrashort time to echo magnetic resonance techniques for the musculoskeletal system. Quant Imaging Med Surg 2016;6(6):731-743. doi: 10.21037/qims.2016.12.06

